Size Dependence of Resistive Switching at Nanoscale Metal-Oxide Interfaces

*Jiechang Hou, Stephen S. Nonnenmann, Wei Qin, and Dawn A. Bonnell**

Size dependent variations in resistive switching using a metal-semiconducting oxide model to examine the underlying mechanisms are reported. In the range of 20 nm to 200 nm, Au nanoparticle/$SrTiO_3$ interface transport properties are size dependent. The size dependence is attributed to the combination of geometric scaling and size-dependent Schottky properties. After electroforming, the observed "eight-wise" bipolar resistive hysteresis loop is modulated by trap/detrap process. The size-dependent high resistance state is consistent with changes in both the interfacial area and Schottky properties. The low resistance state exhibits size independent resistance through the dominant fast conductive path. Detrapping requires more work for smaller interfaces due to the associated larger built-in electric field.

1. Introduction

As device miniaturization advances, existing materials are reaching physical limits, motivating research into new approaches to device function. Resistive switches based on metal oxides are being considered for logic and memory applications.[1–4] The potential for facile device processing and excellent properties has driven recent research on switching mechanisms. The function of a resistive switch is based on the Schottky barrier between a metal and a semiconducting oxide that responds to a voltage by dramatically changing resistance.[5] The mechanism for the dramatic change in resistance varies depending on the materials system and is still under debate in many cases. Processes such as filamentary networks of oxygen vacancies[6] and/or dislocations,[7–9] modification of the interface barrier by trapped charges,[10,11] diffusion of defects[12,13] are invoked.

Interfaces between oxides such as $SrTiO_3$ (STO) and metal electrodes have demonstrated promising resistive memory properties, both in thin film[10,14,15] and bulk systems.[7,27] Metal/oxide nanostructures display a variety of properties depending on the fabrication process or activation method used. Stable unipolar switching,[10] bipolar switching[7,15] and combined responses[16] have been observed, as have different switching directions (clockwise or counterclockwise).[8] As device dimensions approach the nanoscale, interfacial electrical properties dominate, which poses significant implications for efforts to push the limit of crossbar resistive memory design.[12,17,18] At nanometer scale a number of factors can affect electronic transport across an interface.[19–23] Noble metal-$SrTiO_3$ interfaces represent a model system to examine transport across such interfaces.[7,24–27] The Schottky barriers at metal-oxide semiconductor interfaces have been shown to be size dependent for nm-sized clusters[20] and more recently on a larger scale;[28] therefore it might be expected that resistive switching is size dependent.

Conductive atomic force microscopy (CAFM) has been a powerful tool in the study of resistive switching. It can apply a local bias on the substrate surface to probe the lateral homogeneity of oxide thin films and detect local defects via current mapping. Recently, it has been used to verify the presence of highly conductive filaments after electroforming.[8,29,30] The conductive tip can also function as an electrode to measure the electronic properties of nano-sized resistive building blocks. Here, we use the Au nanoparticle/single-crystalline $SrTiO_3$ interface model system to examine the factors that affect resistive switching at nm-sized interfaces. All Au nanoparticle/STO structures exhibit counterclockwise bipolar switching. We show that interface-controlled switching properties are size dependent in the extended range of 20–200 nm.

2. Experimental Results and Discussion

2.1. Interfacial Structures

Interfaces between gold and Nb-doped $SrTiO_3$ (0.02 at%, 6.7×10^{17} cm^{-3}) single crystals with constrained orientation relationships, atomically abrupt interfaces, and sizes ranging from 20–200 nm were fabricated. Al thin films (100 nm) were thermally evaporated on the back of the STO substrate, forming Au nanoparticle/STO/Al structures. **Figure 1**a shows representative topographic images of Au nanoparticles on the atomically smooth $SrTiO_3$(100) surface, where both sizes and morphologies of the nanostructures are observed. Steps of unit cell

---

J. Hou, Prof. D. A. Bonnell
Department of Materials Science and Engineering
University of Pennsylvania
Philadelphia, PA 19104, USA
E-mail: bonnell@lrsm.upenn.edu
Prof. S. S. Nonnenmann
Department of Mechanical and Industrial Engineering
University of Massachusetts
Amherst, MA 01003, USA
W. Qin
Department of Chemical Engineering and Materials Science
University of California
Davis, CA 95616, USA

DOI: 10.1002/adfm.201304121

© 2014 WILEY-VCH Verlag GmbH & Co. KGaA, Weinheim

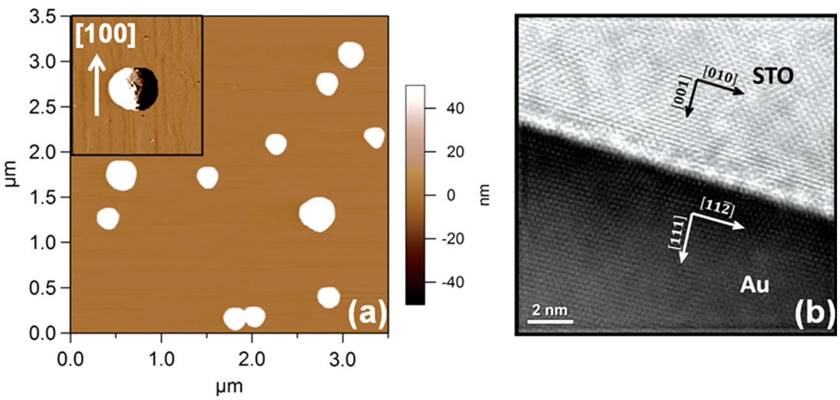

Figure 1. a) A non-contact topographic image of a Au (100)/STO (100) interface. Inset: the [100] orientation is indicated. b) A high resolution TEM image of Au (111)/STO (100), showing a clear abrupt interface. The incident electron beam is parallel to STO [100] and Au [110] simultaneously.

height are measured to be ≈4 nm, typical of atomically abrupt surfaces.[31] Two distinct orientation relationships between the particle and substrate result from surface energy reduction during the high temperature processing.[32,33] The relation between the particle shape and the orientation of the substrate constrains the interface orientation; only Au(111)/STO(100) and Au(100)/STO(100) interfaces are examined here. High resolution transmission electron microscopy (HRTEM) image of a Au(111)/STO(100) interface (Figure 1b) illustrates the structural characteristics observed at all interfaces. The arrows on either side of the interface indicate the orientation relationship between Au nanoparticles and the STO substrate. The $SrTiO_3$ (001) surface is faceted and terminates within a lattice spacing of the surface, parallel to (111) plane of the Au nanoparticle. The interface is atomically abrupt without any contaminant or interface phase. This indicates that the annealing process facilitates the formation of intimate interfaces. Dislocations are sometimes observed along the Au/STO interfaces (Figure S3, Supporting Information).

2.2. Transport Mechanism

A typical current-voltage (*I*–*V*) response from Au nanoparticle/STO/Al structure is shown in **Figure 2**a. The sweeping voltage (±10 V, 0.2 Hz) was applied across the sandwich structure, with the Al bottom electrode grounded. The cut-off observed at larger current ($I >$ 2 nA) is attributed to the built-in amplifier protection, while the plateau near $V = 0$ is due to the amplifier resolution limit. Convention defines the high resistance state (HRS) and low resistance state (LRS) as the lower and higher branch in the hysteresis loops. Applying a positive bias to the Au nanoparticle switches the HRS to the LRS, while negative biases switch the LRS back to the HRS, as indicated by the arrows in Figure 2a. An electroforming process occurs within the first cycle, as indicated by a significant increase in the current (from pA to nA). The electroforming threshold voltage exhibits no correlation with the interface size. Possible explanations for the electroforming threshold include the radiative nature of the electric field through the substrate shadowed by the nano-contact and inhomogeneous defect distribution within the STO substrate, which subsequently contributes to the filament formation.

Figure 2b shows a representative complete *I*–*V* hysteresis loop, with the inset displaying the ln*I*–ln*V* relation for the HRS. A detailed consideration of the current response of the HRS under positive bias shows two regimes. In the low voltage regime from the current-detection limit (0.1 pA) to ≈ 1.5 V, the response demonstrates an exponential dependence on voltage, corresponding to the thermionic emission model,[34]

$$I = AJ_0,\ J_0 = A^*T^2 e^{-\frac{q\Phi_B}{k_BT}}\left(e^{\frac{qV}{nk_BT}} - 1\right) \tag{1}$$

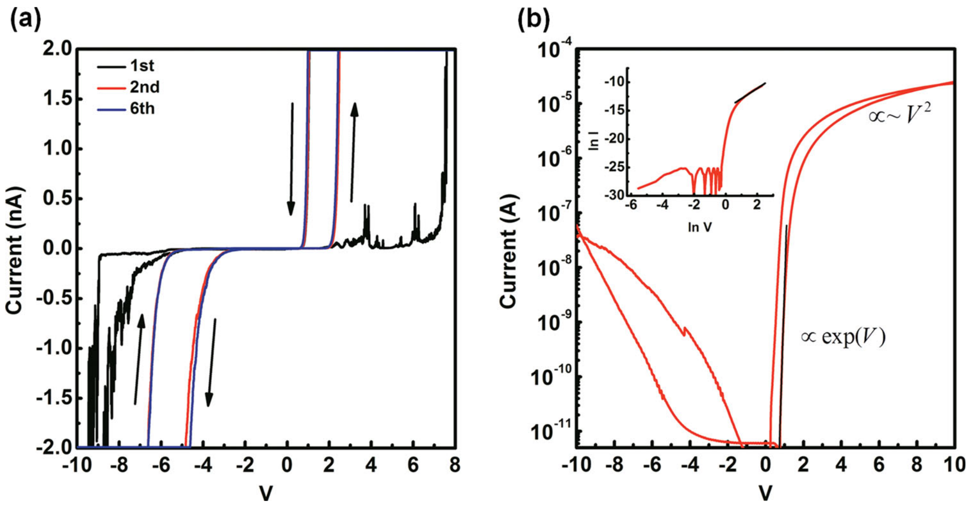

Figure 2. a) Typical hysteresis loops for different cycles. Electroforming occurs at the first cycle followed by stable hysteresis. b) A representative complete *I*–*V* hysteresis loop within ±10 V for a 140 nm Au/STO interface. The inset shows the ln *I*–ln*V* plot for the HRS. The fitting in the smaller and larger applied bias regimes are indicated by solid black lines.

© 2014 WILEY-VCH Verlag GmbH & Co. KGaA, Weinheim

where I is the current, V is the applied voltage, J_0 is the current density, T is the temperature, A is the interfacial area, A^* is the Richardson constant, Φ_B is the Schottky barrier, and n is the ideality factor. As the Au/STO interface size increases, the apparent Φ_B increases and n decreases, dictated by size dependent contributions of edge-induced tunneling and depletion region development.[35] (Examples of measurements obtained with detection at significantly lower currents superimpose on those in the range shown here, confirming that the analysis is valid in this regime, see Figure S2, Supporting Information.)

At higher voltages, the I–V relation deviates from exponential dependence, indicating a transition in transport mechanisms. In the larger bias regime, from 2.5 V to 10 V, there is a clear linear dependence in the $\ln I$–$\ln V$ plot (Figure 2b, inset), with a slope of ≈ 2, indicating that transport is space charge limited current (SCLC).[36] In this regime electron transport is determined by the STO bulk processes rather than the Au/STO interface. The cycle is completed when the applied bias is reversed and the HRS switches to the LRS.

2.3. Switching Mechanism

The effect of size on resistive switching is illustrated in a comparison of the hysteretic I–V responses of various sized Au nanoparticle/STO interfaces (**Figure 3**). All measurements were acquired after the electroforming process to avoid any bulk resistance contributions. The electroforming significantly decreases the bulk resistivity, presumably by forming a network of “filaments” or highly conductive pathways between the top and bottom electrodes. An estimation of bulk STO resistance shadowed by the nanosized top electrode is on the order of 10^{12} Ω (Supporting Information),[37] which would produce current on the order of pA, much lower than that shown in Figure 2. In addition, control measurements of an Al/STO/Al structure showed that the resistance after electroforming is 5 to 6 orders of magnitude lower than the estimated bulk value (Supporting Information). Such conductive paths have been shown to consist of oxygen vacancies prevailing in dislocation defects or crystallographic shear planes.[38,39] Consequently, the activated STO bulk region (or conductive path) shadowed by the nanoparticles resembles an effective bottom electrode with the switching mechanism operating in a region near the interface.

The hysteresis cycles are stable and reproducible (≈20 cycles) (Figure 3a–j), exhibiting “eight-wise” (counterclockwise) behavior for all sweeping amplitudes.[8,40] This behavior is not consistent with the traditional switching mechanism based on filament formation and disruption, which results in “counter eight-wise” (clockwise) behavior.[1,38] One non-filamentary mechanism involving “eight-wise” homogeneous switching results from oxygen vacancy migration, where under negative bias a depletion region forms at the bottom electrode as vacancies migrate towards the top electrode, resulting in switching from the LRS to the HRS.[8] This mechanism might operate in thin films but is unlikely for our system where the physical electrodes are separated by 0.5 mm. A mechanism based on bottom electrode interactions is also unlikely to be size dependent, in contrast to Figure 3a–j that exhibits a clear size trend in hysteresis width. Diffusion of the Al bottom electrode induced by an electrochemical reaction is similarly implausible.

Figure 3k illustrates the typical resistive switching in these samples, displaying both the HRS (black) and LRS (red), which we describe in terms of interface trapping. The trap sites are oxygen vacancies near the interface and/or undercoordinated Ti sites at the interface. These bonding configurations are known to trap electrons[10] and electron energy loss spectroscopy (EELS) profiles across the interface show an increase in reduced Ti atoms in this interface region (see Figure S3, Supporting Information). Here, the Schottky barrier at the top electrode has two major effects. 1) The built-in electric field induces aggregation of defect states, providing a possible source of trap states in the vicinity of the interface region. 2) The Schottky barrier dictates electron transport mechanisms. As the junction scales down to sub-100 nm, thermionic emission and tunneling coexist. Whether tunneling is favored near the Schottky region determines the resistance states in this case. When the metal nanoparticle is negatively biased, electrons can occupy the lower energy trap states in the vicinity of interface region, creating a Coulombic barrier to electron transport, blocking the tunneling path. As the negative bias on the nanoparticle increases (Figure 3k, inset, left), a larger fraction of interface traps become occupied, thus impeding current flow and the system switches to the HRS.[37,40–42] Conversely, under positive bias (Figure 3k, inset, right), detrapping occurs, which enables electron transport by trap-assisted tunneling in addition to thermionic emission and results in the LRS. The vicinity in which the trapping occurs can be on the order of nms, similar in the dimension to thin film devices.

2.4. Size Dependent Hysteresis

Figure 3 shows that the switching hysteresis is clearly size dependent for both Au(100)/STO(100) (Figure 3a–e) and Au(111)/STO(100) (Figure 3f–j) interfaces. Although complete hysteresis loops are not obtained due to the instrument limitations for measurements of such small interfaces, it is clear that the apparent voltage for the HRS-to-LRS transition at positive bias increases with decreasing interface size for both cases.

Figure 4 quantifies this trend by comparing the size dependence of resistance at a constant voltage. The HRS resistances for both interfaces were extrapolated to a read-out voltage of 1 V based on the thermionic emission fitting (Supporting Information). It is clear that the HRS and LRS possess different size dependence behaviors. We believe that this difference of size dependence lies in whether the interface traps are filled or not and the associated contributing transport mechanisms. For both Au(100)/STO(100) (Figure 4a) and Au(111)/STO(100) (Figure 4b) interfaces, the LRS resistance appears to be independent of the interface size. Charge detrapping at the interface enables tunneling to the bulk region with reduced resistivity caused by electroforming, which is size independent. The resistance of the high resistance states, however, exhibits a strong size dependence for both interfaces. As indicated by Equation 1, there is an explicit area dependence in the transport. The question at issue here is whether the current density J_0 is inherently size dependent at the nano-scale. The blue

© 2014 WILEY-VCH Verlag GmbH & Co. KGaA, Weinheim

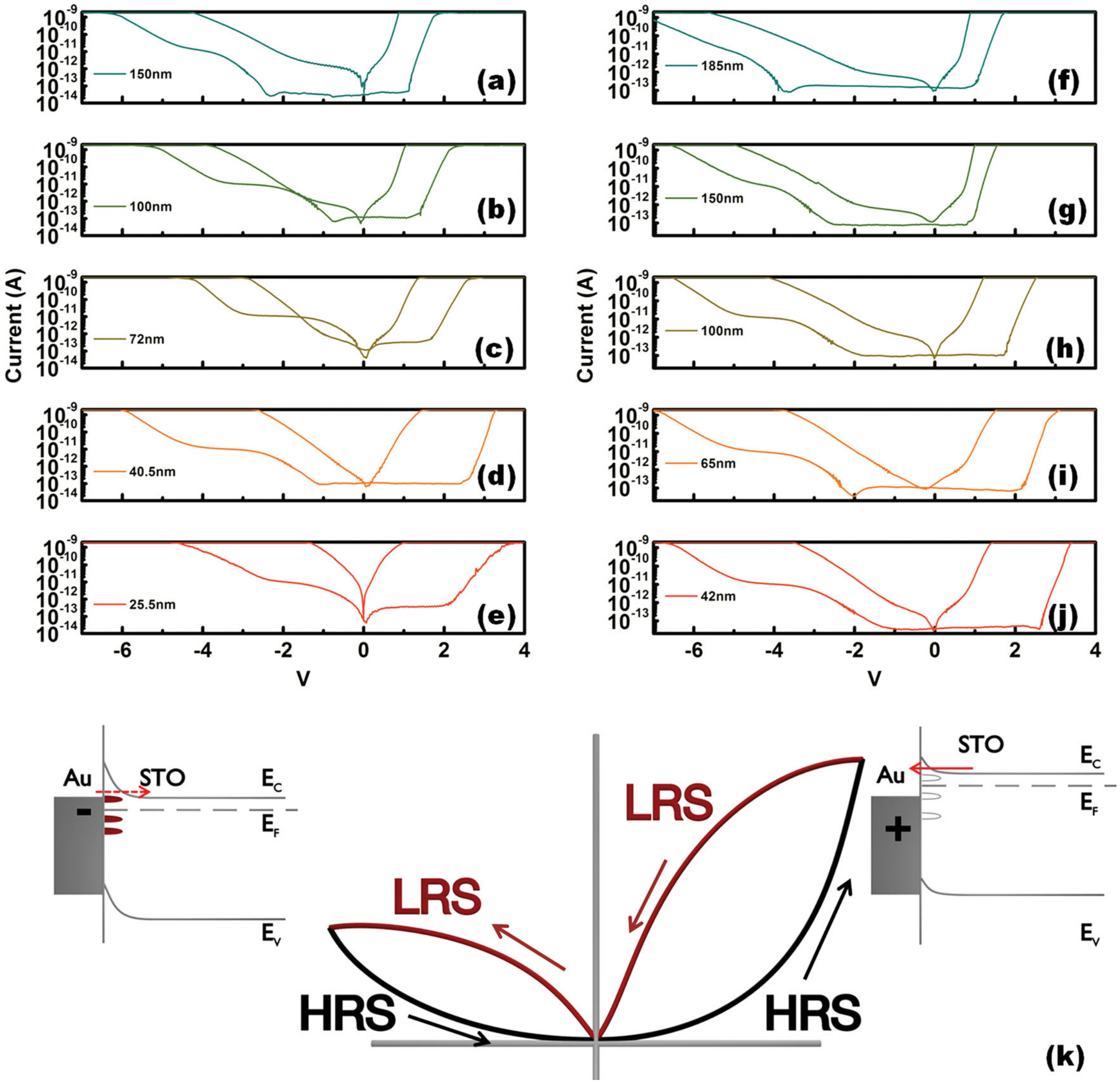

Figure 3. a–e) Representative logscale *I*–*V* response of individual Au(100)/STO(100) interfaces with decreasing size. f–j) Logscale *I*–*V* response of individual Au(111)/STO(100) interfaces with decreasing size. k) Schematic illustration of a typical resistive switching *I*–*V* response in logscale, displaying both an HRS (black) and LRS (red) state. Arrows indicate the switching direction. Inset: band diagrams for the detrapping (positive bias; HRS → LRS) process and trapping (negative bias; LRS → HRS) process. Dashed arrow from Au to STO represents weakened tunneling during trapping.

line in Figure 4 extrapolates the geometric effect on measured resistance. Clearly for both types of interfaces, the observed increase is significantly more than that due to the decreasing area at interfaces with diameters less than ≈100 nm, indicating that there is an additional size dependence in J_0. This contribution to the size dependence must be mechanistic in nature. As noted earlier, Φ_B and n exhibit size dependence due to edge-related field effects in mid-ranged sizes and inhomogeneity at the smallest sizes.[35] This, however, does not explain the switching behavior. Note that the built-in electric field at the interface is highly size dependent and opposite in sign to the external field applied to induce the HRS to LRS switching. It is reasonable that a larger applied voltage is required to depopulate the traps.

The area of the switching hysteresis loop is generally associated with a dissipation energy.[44] Although the data in Figure 3 do not contain complete hysteresis loops, it is clear that the associated energy increases with decreasing interface size. We illustrate this trend by comparing the energy derived from the hysteresis loop areas within the range measured, as shown in **Figure 5**.[45] This approach does not yield the absolute value of the energy. But since the measurements were in the same bias ramp range, it semi-quantitatively depicts the size dependence trend. The loop area analysis in Figure 5 indicates that there is an increase in energy of 2.5–3.5 times as interface diameter decreases from ≈150 nm to ≈20 nm. This increase is consistent with the presence of a higher built-in field below the smaller interfaces. Alternatively, this local field, which would be present during sample annealing, could have caused a variation in the local defect concentration. Previous studies have successfully manipulated resistance loops by using ion implantation to produce additional traps.[46] Our results can not distinguish between these two possibilities, but both are a consequence of the the size dependence of local electric fields.

© 2014 WILEY-VCH Verlag GmbH & Co. KGaA, Weinheim

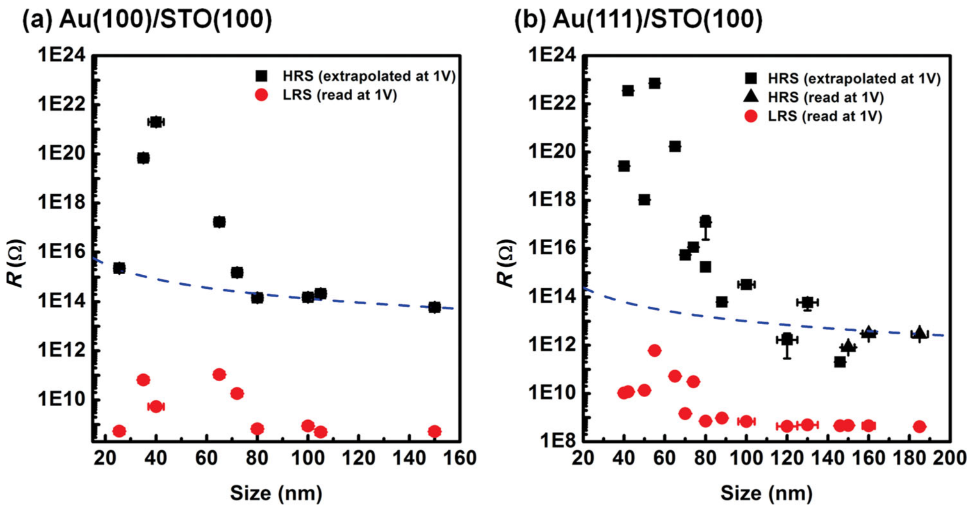

Figure 4. Resistance of the LRS and the HRS for a) (100) interfaces and b) (111) interfaces of various sizes, at 1 V. The blue dashed lines scale the resistance with the largest interface by contact area, i.e., 150 nm contact for (100) interface and 185 nm contact for (111) interface. Here, the simple linear areal scaling of resistance fails at the nanometer regime.

3. Conclusions

In conclusion, for the case of resistive switching transitions based on charge trapping mechanisms, the switching is shown to exhibit size dependence. In addition to the geometric scaling of resistance, this size dependence of switching response is concomitantly determined by the size-dependent interface Schottky barriers and can be attributed to the local electric field effects.

4. Experimental Section

Fabrication: Single crystal Nb-doped $SrTiO_3$(100) (Princeton Scientific, 5 mm × 5 mm × 0.5 mm) substrates with dopant concentration 0.02 at% were cleaned with acetone and ethanol by sonication. Then the substrates were annealed at 1000 °C for 1 h to obtain a flat clean surface. Commercially available gold nanoparticles (citrate stabilized in H_2O solution, British Biocell) of various diameters (20/40/60/100/150 nm) were deposited on the substrates at 110 °C on the hot plate. Au nanoparticles remained dispersed on the surface after the solution was boiled away. Samples were annealed at 950 °C for an hour to remove surface ligands and form intimate contacts. Afterwards, a 100 nm film of aluminum was thermally evaporated on the back side of the samples to form Ohmic contacts. The Au/STO/Al stacked structures were silver-pasted on an AFM mount.

Electrical Measurements: Samples were imaged in AC tapping mode (Asylum MFP-3D AFM). The particle shapes can be determined from topographic images, while particle sizes were estimated from the height profiles. In contact mode (ORCA), the Pt-coated conductive tip (Olympus AC240TM) was engaged on individual nanoparticles. Only completely-facetted particles were tested. The current-voltage (*I–V*) curves were obtained from −10 V to 10 V for at least 8 cycles each, producing 8 measurements of the interface properties. A force analysis was performed to optimize the intimate tip-particle electrical contact without damage and forces were limited to 10 nN.[43] Particles were imaged after each electrical characterization. Any particle exhibiting

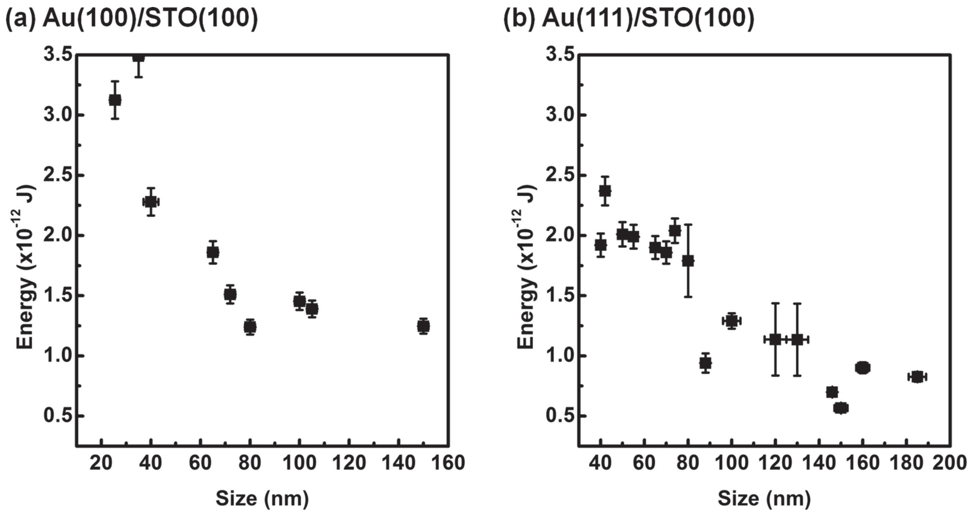

Figure 5. The energy within the hysteresis loop for a) Au(100)/STO(100) and b) Au(111)/STO(100) interfaces.[45]

damage was not considered in the analysis. To obtain a complete hysteresis loop, a home-made external amplifier was connected into the machine circuit.

TEM Imaging: The Au nanoparticles were extremely small, about 100 nm in diameter, so the electron transparent cross-sections were prepared by focused ion beam (FIB) lift-out method. A FEI Strata DB235 FIB was used to extract a section through the center of a nanoparticle and the final thinning was performed using a 5 kV ion beam in order to minimize the damage. HRTEM analysis was carried out on JEOL 2100 TEM with 200 kV accelerating voltage, and a vacuum of less than 3×10^{-5} Pa. Digital Micrograph software from Gatan was used to perform the image processing.

Supporting Information

Supporting Information is available from the Wiley Online Library or from the author.

Acknowledgements

This work was supported by the Department of Energy, Office of Basic Energy Science (DE-FG02–00ER45813) with facilities support by the Nano/Bio Interface Center (grant DMR08–32802) and the Laboratory for Research on the Structure of Matter (grant DMR11–20901). The authors are grateful for insightful discussions with J. Santiago, as well as the assistance of Graham Wabiszewski, Xiang Yang, E. Ashley Gaulding, Elaine Lee, and Kagan Group in macroscopic electronic measurements.

Received: December 9, 2013
Revised: January 28, 2014
Published online: March 26, 2014

---

[1] R. Waser, R. Dittmann, G. Staikov, K. Szot, *Adv. Mater.* **2009**, *21*, 2632.
[2] R. Waser, M. Aono, *Nat. Mater.* **2007**, *6*, 833.
[3] K. M. Kim, D. S. Jeong, C. S. Hwang, *Nanotechnology* **2011**, *22*, 254002.
[4] A. Sawa, *Mater. Today*, **2008**, *11*, 28.
[5] J. J. Yang, M. D. Pickett, X. Li, D. A. A. Ohlberg, D. R. Stewart, R. S. Williams, *Nat. Nanotechnol.* **2008**, *3*, 429.
[6] S. S. Nonnenmann, E. M. Gallo, J. E. Spanier, *Appl. Phys. Lett.* **2010**, *97*, 102904.
[7] K. Szot, W. Speier, G. Bihlmayer, R. Waser, *Nat. Mater.* **2006**, *5*, 312.
[8] R. Muenstermann, T. Menke, R. Dittmann, R. Waser, *Adv. Mater.* **2010**, *22*, 4819.
[9] D. S. Jeong, R. Thomas, R. S. Katiyar, J. F. Scott, H. Kohlstedt, A. Petraru, C. S. Hwang, *Rep. Prog. Phys.* **2012**, *75*, 076502.
[10] D. Choi, D. Lee, H. Sim, M. Chang, H. Hwang, *Appl. Phys. Lett.* **2006**, *88*, 082904.
[11] A. B. K. Chen, S. G. Kim, Y. Wang, W. Tung, I. Chen, *Nat. Nanotechnol.* **2011**, *6*, 237.
[12] J. Sullaphen, K. Bogle, X. Cheng, J. M. Gregg, N. Valanoor, *Appl. Phys. Lett.* **2012**, *100*, 203115.
[13] S. Choi, G. Park, K. Kim, W. Yang, H. Bae, K. Lee, H. Lee, S. Y. Park, S. Heo, H. Shin, S. Lee, S. Cho, *J. Appl. Phys.* **2011**, *110*, 056106.
[14] S. Menzel, M. Waters, A. Marchewka, U. Böttger, R. Dittmann, R. Waser, *Adv. Funct. Mater.* **2011**, *21*, 4487.
[15] Ch. Lenser, A. Kuzmin, J. Purans, A. Kalinko, R. Waser, R. Dittmann, *J. Appl. Phys.* **2012**, *111*, 076101.
[16] X. Sun, G. Li, X. Zhang, L. Ding, W. Zhang, *J. Phys. D: Appl. Phys.* **2011**, *44*, 125404.
[17] T. Yanagida, K. Nagashima, K. Oka, M. Kanai, A. Klamchuen, B. H. Park, T. Kawai, *Sci. Rep.* **2013**, *3*, 1657.
[18] Q. Xia, M. D. Pickett, J. J. Yang, X. Li, W. Wu, G. Medeiros-Ribeiro, R. S. Williams, *Adv. Funct. Mater.* **2011**, *21*, 2660.
[19] G. D. J. Smit, S. Rogge, T. M. Klapwijk, *Appl. Phys. Lett.* **2002**, *81*, 3852.
[20] D. A. Bonnell, Y. Liang, M. Wagner, D. Carroll, M. Rühle, *Acta Mater.* **1998**, *46*, 2263.
[21] J. L. Tedesco, J. E. Rowe, R. J. Nemanich, *J. Appl. Phys.* **2009**, *105*, 083721.
[22] D. L. Carroll, M. Wagner, M. Rühle, D. A. Bonnell, *Phys. Rev. B* **1997**, *55*, 9792.
[23] F. Léonard, A. A. Talin, *Phys. Rev. Lett.* **2006**, *97*, 026804.
[24] H. Hasegawa, T. Nishino, *J. Appl. Phys.* **1991**, *69*, 1501.
[25] T. Shimizu, N. Gotoh, N. Shinozaki, H. Okushi, *Appl. Surf. Sci.* **1997**, *117*, 400.
[26] T. Shimizu, H. Okushi, *J. Appl. Phys.* **1999**, *85*, 7244.
[27] X. T. Zhang, Q. X. Yu, Y. P. Yao, X. G. Li, *Appl. Phys. Lett.* **2010**, *97*, 222117.
[28] R. Kraya, L. Y. Kraya, D. A. Bonnell, *Nano Lett.* **2010**, *10*, 1224.
[29] L. Yang, C. Kuegeler, K. Szot, A. Ruediger, R. Waser, *Appl. Phys. Lett.* **2009**, *95*, 013109.
[30] X. Chen, N. Wu, J. Strozier, A. Ignatiev, *Appl. Phys. Lett.* **2006**, *89*, 063507.
[31] D. A. Bonnell, J. Garra, *Rep. Prog. Phys.* **2008**, *71*, 044501.
[32] L. Vitos, A. V. Ruban, H. L. sSkriver, J. Kollár, *Surf. Sci.* **1998**, *411*, 186.
[33] J. Shim, B. Lee, Y. W. Cho, *Surf. Sci.* **2002**, *512*, 262.
[34] S. M. Sze, K. K. Ng, *Physics of Semiconductor Devices*, 3rd Edition, Wiley, Hoboken, NJ, USA **2007**.
[35] J. Hou, S. S. Nonnenmann, W. Qin, D. A. Bonnell, *Appl. Phys. Lett.* **2013**, *103*, 252106.
[36] A. Rose, *Phys. Rev.* **1955**, *97*, 1538.
[37] T. Fujii, M. Kawasaki, A. Sawa, Y. Kawazoe, H. Akoh, Y. Tokura, *Phys. Rev. B* **2007**, *75*, 165101.
[38] D. Kwon, K. M. Kim, J. H. Jang, J. M. Jeon, M. H. Lee, G. H. Kim, X. Li, G. Park, B. Lee, S. Han, M. Kim, C. S. Hwang, *Nat. Nanotechnol.* **2010**, *5*, 148.
[39] J. J. Yang, D. B. Strukov, D. R. Stewart, *Nat. Nanotechnol.* **2013**, *8*, 13.
[40] K. Shibuya, R. Dittmann, S. Mi, R. Waser, *Adv. Mater.* **2010**, *22*, 411.
[41] A. Sawa, T. Fujii, M. Kawasaki, Y. Tokura, *Appl. Phys. Lett.* **2004**, *85*, 4073.
[42] S. Fleischer, P. T. Lai, Y. C. Cheng, *J. Appl. Phys.* **1992**, *72*, 5711.
[43] J. Hou, B. Rouxel, W. Qin, S. S. Nonnenmann, D. A. Bonnell, *Nanotechnology* **2013**, *24*, 395703.
[44] Y. M. Lu, M. Noman, Y. N. Picard, J. A. Bain, P. A. Salvador, M. Skowronski, *J. Appl. Phys.* **2013**, *113*, 163703.
[45] The energy within the loop is calculated by the integration of the HRS branch subtracted by that of the LRS branch, multiplied by time interval ($\Delta t = 5 \times 10^{-4}$ s) between two data points, where $E = \sum_i \{P_i \Delta t\} = \sum_i \{I_i V_i \Delta t\} = \Delta t \int \{I(V) \mathrm{d}V\}$.
[46] Q. Liu, W. Guan, S. Long, R. Jia, M. Liu, J. Chen, *Appl. Phys. Lett.* **2008**, *92*, 012117.

© 2014 WILEY-VCH Verlag GmbH & Co. KGaA, Weinheim